ARTICLE NO. 80-4094

C 80-114

# Higher Order Farfield Drag Minimization for a Subcritical Wing Design Code

00001
20016

J. M. Kuhlman*
*Old Dominion University, Norfolk, Va.*

**A higher order Trefftz plane model of the undistorted interacting wing wakes of two symmetric subsonic planforms has been developed and integrated with an existing vortex lattice wing design code. The Trefftz plane calculation provides continuous, piecewise quadratically varying bound circulations, which are then interpolated in the nearfield vortex lattice representation of the wing. Integration of the surface slopes for a specified chord loading function provides the design wing camber surfaces. This paper outlines the theoretical development and presents comparisons between results obtained using the present theory and 1) previous exact solutions for minimum induced drag and 2) previous wing designs obtained using a discrete vortex wake model.**

## Nomenclature

| | |
|---|---|
| $a$ | = chord load function shape, as defined in Fig. 11 |
| $A$ | = aspect ratio |
| $A_{ij}$ | = element of matrix of coefficients in the induced drag Eqs. (21) and (22) |
| AIC | = aerodynamic influence coefficient |
| $b$ | = wing span |
| $C_B$ | = wing root bending moment coefficient |
| $C_D$ | = induced drag coefficient |
| $C_L$ | = lift coefficient |
| $C_m$ | = pitching moment coefficient |
| $c$ | = local chord |
| $\bar{c}$ | = reference wing chord |
| $c_l$ | = section lift coefficient |
| $d$ | = maximum vertical extent of wings of Ref. 13 |
| $G_i, \bar{G}_i, \hat{G}_i$ | = variables containing the unknown wake vortex sheet strengths, appearing in drag and bound circulation Eqs. (9) and (4) |
| $h_{ij}$ | = distance between influenced point on panel $i$ and influencing point on panel $j$ |
| $h'_{ij}$ | = distance between influenced point on panel $i$ and influencing point on image of panel $j$ |
| $H$ | = gap between biplane wings |
| $I_{1ij}, I_{2ij}, I_{3ij}, I_{4ij}, I_{5ij}, I_{6ij}$ | = influence coefficient integrals appearing in induced drag Eq. (9) |
| $k$ | = induced drag efficiency parameter, defined as $C_L^2/(C_D \pi A)$ |
| $l$ | = vertical extent of endplate or fractional semispan of upper wing of biplane |
| $M$ | = Mach number |
| $N$ | = total number of wake panels |
| $R_{ij}$ | = projection of distance $h_{ij}$ onto the plane of influenced panel $i$ |
| $R'_{ij}$ | = projection of distance $h'_{ij}$ onto the plane of influenced panel $i$ |
| $S$ | = reference wing area |
| $s$ | = wake panel semiwidth |
| $s$ | = local wake panel coordinate |
| $U$ | = freestream speed |
| $w_n$ | = normal wash velocity |
| $w_0$ | = constant appearing in Munk's criterion normal wash expression, Eqs. (15) and (16) |
| $x$ | = streamwise body axis coordinate |
| $x_c$ | = $x$ coordinate of center of pressure |
| $\Delta x$ | = shift of pitching moment reference |
| $XP, XM$ | = terms in Eq. (12) containing $x_c$, as defined in Eqs. (13) and (14) |
| $y$ | = spanwise body axis coordinate |
| $z$ | = vertical body axis coordinate |
| $z_c$ | = vertical separation between two planforms in Figs. 14-16 |
| $\beta = 2d/b$ | = parameter for circular arc spanwise camber wings of Ref. 13 |
| $\gamma$ | = wing wake vortex sheet strength |
| $\Gamma$ | = bound circulation |
| $\Gamma_0(-s_i)$ | = bound circulation at outboard end of wake panel $i$ |
| $\epsilon$ | = incidence angle |
| $\eta$ | = nondimensional wing semispan |
| $\lambda$ | = Lagrange multiplier |
| $\xi$ | = local fractional chordwise coordinate |
| $\phi$ | = dihedral angle |

## Introduction

THE current goal of improving the fuel efficiency of transport aircraft may, in part, be achieved through a careful design of the aerodynamic surfaces for attached flow and minimum induced drag. Many previous authors have developed potential flow wing design or analysis codes based upon a vortex lattice representation of the aerodynamic surfaces; e.g., see Refs. 1-5. Such codes using this relatively simple theoretical model are useful for preliminary design purposes. However, both Lamar[1] and Feifel[3] note that vortex lattice methods predict induced velocities which are in error in the vicinity of a change in the wing dihedral. These localized errors in induced velocities apparently do not lead to appreciable errors in overall coefficients, but vortex lattice design camber shapes in the vicinity of changes in wing dihedral may, as a result, be in error.

To improve the accuracy of the induced velocity computation, the current work uses a two-dimensional advanced panel model of the wakes of two interacting planforms to minimize and compute the induced drag in the Trefftz plane. The wake vortex sheet strengths are assumed to vary piecewise linearly. Similar aerodynamic modeling techniques have recently been used by Clever[6] and Goldhammer[7] in three-dimensional subsonic analysis codes. Both of these references

Received July 30, 1979; revision received Jan. 28, 1980. 

Index categories: Aerodynamics; Subsonic Flow.

*Associate Professor, Dept. of Mechanical Engineering and Mechanics. Member AIAA.

assume a piecewise linearly varying chord loading. Loth and Boyle[8] give the theoretical development for a wing wake model where the wing shed vortex sheet strength is assumed to vary piecewise linearly. A Trefftz plane analysis is performed, and Munk's criterion[9] is used to develop expressions which lead to the wake vorticity distribution for minimum induced drag. However, the numerical results presented in Ref. 8 do not agree with available exact solutions for induced drag of nonplanar configurations.[10-13] This is believed to be due to errors in the computer code of Ref. 8.

In the current work, a Trefftz plane analysis for multiple interacting subsonic planforms has been performed, using the basic theoretical model developed in Ref. 8. Advancements of the current method include the following: 1) the current theory and code allows the use of variable-sized wake segments; 2) logarithmic singularities at the wing tip and adjacent wake panels are currently treated differently than in Ref. 8; 3) the farfield induced drag is calculated analytically by integration of the product of induced normal velocity and bound circulation; 4) a direct optimization technique has been developed and compared with the Munk criterion optimization procedure; and 5) expressions for the wing root bending moment and pitching moment have been developed so that constrained, trimmed configurations may be analyzed. The theoretical development has been described in Ref. 14, but is outlined in the current paper for completeness. Minimum induced drag solutions obtained using the current theory are next compared with the exact solutions of Refs. 10-13 for single and multiple planforms. Finally, two examples of wing designs using the current Trefftz plane theory are presented. These wing camber surfaces have been obtained using a newly developed wing design code which utilizes the geometry and surface slope integration sections of the code described in Ref. 1, mated with the current wake model and optimizer. These results are compared with camber shape designs for the same planforms obtained using the original design code of Ref. 1.

## Development of Trefftz Plane Theory

An expression for the induced drag for multiple interacting subsonic planforms is developed from the standard equation for induced drag evaluated in the farfield, in coefficient form:

$$C_D = \frac{1}{S}\int_{-b/2}^{b/2} \frac{w_n(\delta)}{U}\frac{\Gamma(\delta)}{U}\frac{\mathrm{d}\delta}{\cos\phi} \tag{1}$$

Expressions for the individual components of the integrand are developed as follows. Following the theoretical model of Loth and Boyle[8] the farfield wing wake vortex sheet strength is assumed to vary piecewise linearly with the spanwise coordinate. That is, for each of $N$ variable-sized wake segments, the vortex sheet strength $\gamma$ is

$$\gamma(\delta_i) = \frac{\gamma_{i+1}+\gamma_i}{2} + \frac{\gamma_{i+1}-\gamma_i}{2}\cdot\frac{\delta_i}{s_i}, i = 1,\ldots,N \tag{2}$$

The undistorted wake geometry for a single planform, viewed looking upstream, is shown in Fig. 1. Here $\delta_i = 0$ corresponds to the center of wake segment $i$, and $s_i$ is the wake segment halfwidth. Wake segments are numbered sequentially for the left half of the planform beginning at the tip. The vortex sheet strength between wake segments $i-1$ and $i$ is denoted by $\gamma_i$. It has been shown in Ref. 14 that analytical expressions for the induced normal velocities in the Trefftz plane at an arbitrary point on the wake segment $i$ due to wake segment $j$ and its image are, using the law of Biot-Savart,

$$w_{n,j}(\delta_i) = \frac{1}{2\pi}\int_{-s_j}^{s_j}\gamma(\delta_j)\left(\frac{R_{ij}}{h_{ij}^2} - \frac{R'_{ij}}{h'^2_{ij}}\right)\mathrm{d}\delta_j \tag{3}$$

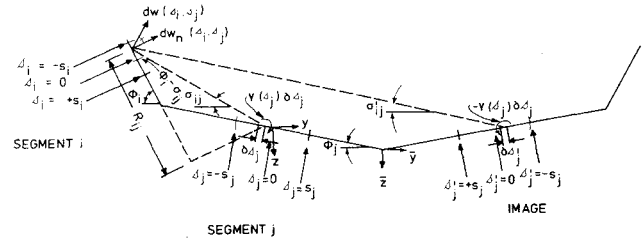


**Fig. 1 Trefftz plane geometry used in present method.**

Here $h_{ij}$ denotes distance between points on segments $i$ and $j$, $R_{ij}$ is the projection of $h_{ij}$ onto the plane containing wake segment $i$, and primes denote corresponding quantities for the image of segment $j$ (see Fig. 1). For the assumed $\gamma$ distribution given by Eq. (2), Eq. (3) is integrated analytically for all $(i,j)$ pairs. Equation (2) is also integrated spanwise to give the bound circulation, which is

$$\frac{\Gamma(\delta_i)}{U} = G_i + \bar{G}_i\delta_i + \hat{G}_i\frac{\delta_i^2}{2s_i} \tag{4}$$

where

$$G_i = \frac{\Gamma_0(-s_i)}{U} + \frac{s_i}{4U}(\gamma_{i+1}+3\gamma_i) \tag{5}$$

$$\bar{G}_i = \frac{\gamma_{i+1}+\gamma_i}{2U} \tag{6}$$

$$\hat{G}_i = \frac{\gamma_{i+1}-\gamma_i}{2U} \tag{7}$$

$$\Gamma_0(-s_i) = \sum_{k=1}^{i-1}\int_{-s_k}^{s_k}\gamma(\delta_k)\,\mathrm{d}\delta_k = \gamma_1 s_1 + \sum_{k=2}^{i-1}\gamma_k(s_k+s_{k-1}) + \gamma_i s_{i-1} \tag{8}$$

Equations (3) and (4), when substituted into the induced drag expression for wake segment $i$ due to segment $j$ and its image, yield

$$C_{D,ij} = (1/S)(G_i\bar{G}_jI_{1ij} + G_i\hat{G}_jI_{2ij} + \bar{G}_i\bar{G}_jI_{3ij} + \bar{G}_i\hat{G}_jI_{4ij} + \hat{G}_i\bar{G}_jI_{5ij} + \hat{G}_i\hat{G}_jI_{6ij}) \tag{9}$$

where $(I_{1ij}, I_{2ij}, I_{3ij}, I_{4ij}, I_{5ij}, I_{6ij})$ are given in Ref. 14. The total induced drag equals twice the sum of $C_{D,ij}$ over all possible values of $i$ and $j$.

The above influence coefficient integrals have been evaluated analytically as detailed in Ref. 14, using the MACSYMA symbolic manipulation language.[15] Logarithmic singularities which occur at the wing tip and at ends of adjacent wake segments have simply been omitted from the integration range. An analytical justification of this procedure has not been found, but numerical studies indicate that the calculated $C_D$ is not affected by the size of the omitted integration range surrounding the singularity from $10^{-3}$ to $10^{-8}$ of the smallest wake segment.[14]

### Aerodynamic Computations

The lift, wing root bending moment, and pitching moment coefficients have been evaluated, utilizing the Kutta-Joukowski law, as:

$$C_L = \frac{8}{S}\frac{1}{3}\sum_{i=1}^{N}\cos\phi_i\left\{s_i^2\left(\frac{\gamma_{i+1}}{U}+\frac{2\gamma_i}{U}\right) + 3s_i\frac{\Gamma_0(-s_i)}{U}\right\} \tag{10}$$

$$C_B = -\frac{2}{Sb}\sum_{i=1}^{N}\left\{(y_i\cos\phi_i + z_i\sin\phi_i)\left(2s_i\frac{\Gamma_0(-s_i)}{U}\right.\right.$$

$$\left.\left.+\frac{4}{3}s_i^2\frac{\gamma_i}{U}+\frac{2}{3}s_i^2\frac{\gamma_{i+1}}{U}\right)+\frac{1}{3}s_i^3\left(\frac{\gamma_{i+1}+\gamma_i}{U}\right)\right\} \quad (11)$$

Here $(y_i,z_i)$ are the coordinates of the center of wake vortex panel $i$.

$$C_m = \frac{2}{Sc}\sum_{i=1}^{N}\cos\phi_i\left\{2s_iXP_i\frac{\Gamma_0(-s_i)}{U}+\frac{1}{3}\frac{\gamma_{i+1}}{U}s_i^2\right.$$

$$\left.(XM_i+2XP_i)+\frac{1}{3}\frac{\gamma_i}{U}s_i^2(XM_i+4XP_i)\right\} \quad (12)$$

The $(XP_i,XM_i)$ are defined in terms of the $x$ coordinates of the center of pressure in the nearfield at the $y$ coordinates corresponding to the centers of wake vortex sheet panels $i$ and $i+1$. That is, for $x_{ci}$ denoting the $x$ coordinate of the wing center of pressure at $y_i$,

$$XP_i = \frac{x_{ci+1}+x_{ci}}{2} \quad (13)$$

$$XM_i = \frac{x_{ci+1}-x_{ci}}{2} \quad (14)$$

For the current work, the $x_{ci}$ coordinates are calculated for a specified member of the NACA a-series mean line chordwise pressure distributions.[16]

## Drag Minimization

Using this model of the wing wakes, two different drag minimization techniques have been implemented: first, use of Munk's criterion[9] for configurations not subjected to any constraints on $C_B$ or $C_m$ and second, a constrained direct optimization technique, such as that described in Refs. 1 and 4. These techniques are now discussed.

### Munk's Method

Munk's criterion states that

$$\frac{w_n}{\cos\phi} = w_0 = \text{constant} \quad (15)$$

at all points on the wing wake. Using this, a system of $N$ equations is developed for the $N$ unknown shed sheet strengths by equating the total normal induced velocity at each wake segment center to $\cos\phi_i$. That is,

$$\cos\phi_i = \frac{1}{2\pi w_0}\sum_{j=1}^{N}\left\{\left(\frac{\gamma_{j+1}+\gamma_j}{2}\right)\left[\int_{-s_j}^{s_j}\frac{R_{ij}}{h_{ij}^2}\,d\delta_j\right.\right.$$

$$-\int_{-s_j}^{s_j}\frac{R'_{ij}}{h_{ij}'^2}\,d\delta_j\Big]+\left(\frac{\gamma_{j+1}-\gamma_j}{2}\right)\left[\int_{-s_j}^{s_j}\frac{\delta_j R_{ij}}{h_{ij}^2 s_j}\,d\delta_j\right.$$

$$\left.\left.-\int_{-s_j}^{s_j}\frac{\delta_j R'_{ij}}{h_{ij}'^2 s_j}\,d\delta_j\right]\right\} \quad (16)$$

To insure symmetric loading, it has been assumed that the wake vortex sheet strength at the centerline $\gamma_{N+1}$ equals zero. The above equations yield the optimum wake vortex sheet distribution for minimum induced drag, scaled by the constant $w_0$. The ratio of $w_0$ to the freestream speed is calculated from a revised form of the lift coefficient Eq. (10):

$$C_L = \frac{8}{S}\left\{\frac{1}{3}\sum_{i=1}^{N}\left[\cos\phi_i s_i^2\left(\frac{\gamma_{i+1}}{w_0}+\frac{2\gamma_i}{w_0}\right)\right]\right.$$

$$\left.+\sum_{i=1}^{N}\cos\phi_i s_i\frac{\Gamma_0(-s_i)}{w_0}\right\}\frac{w_0}{U} \quad (17)$$

Once the optimum $\gamma_i$ values have been rescaled by $w_0/U$, they are utilized to calculate the bound circulation distribution from Eqs. (4-8) and the induced drag coefficient from Eq. (9).

### Direct Optimization

The direct optimization technique evaluates the wake vortex shed sheet distribution using Lagrange multipliers to include $C_L$, $C_m$, and $C_B$ constraints, as needed. The function to be extremized is

$$C_D+\lambda_1\left(\sum_{i=1}^{N}C_{L,i}\frac{\gamma_i}{U}-C_L\right)+\lambda_2\left(\sum_{i=1}^{N}C_{m,i}\frac{\gamma_i}{U}-0\right)$$

$$+\lambda_3\left(\sum_{i=1}^{N}C_{B,i}\frac{\gamma_i}{U}-C_B\right)$$

Here the $C_{L,i}$, $C_{B,i}$, and $C_{m,i}$ denote partial derivatives of the respective coefficients with respect to the quantity $(\gamma_i/U)$. As developed in Ref. 14, the lift coefficient derivative is

$$C_{L,i} = \frac{8}{S}\left\{\frac{2}{3}\cos\phi_i s_i^2+\frac{1}{3}\cos\phi_{i-1}s_{i-1}^2\right.$$

$$\left.+\sum_{m=1}^{N-i}\left(\cos\phi_{m+i}s_{m+i}\right)\left(s_i+s_{i-1}\right)\right\} \quad (18)$$

while the derivatives of $C_m$ and $C_B$ are

$$C_{m,i} = \frac{4}{Sc}\left\{\frac{1}{3}\cos\phi_i s_i^2\left(XM_i+4XP_i\right)+\frac{1}{3}\cos\phi_{i-1}s_{i-1}^2\right.$$

$$\left.\left(XM_{i-1}+2XP_{i-1}\right)\right\}+\frac{8}{Sc}\left\{s_i\cos\phi_i XP_i s_{i-1}+\left(s_i+s_{i-1}\right)\right.$$

$$\left.\sum_{j=i+1}^{N-1}s_j\cos\phi_j XP_j\right\} \quad (19)$$

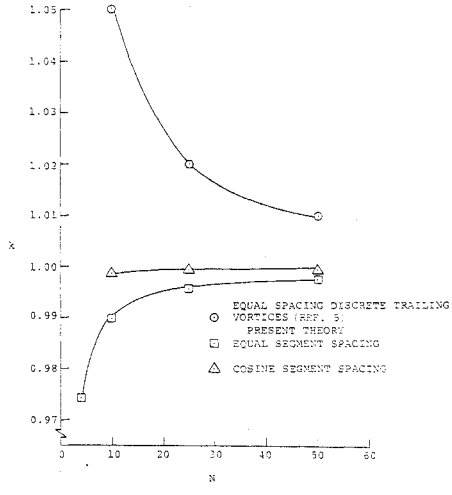


**Fig. 2 Convergence of induced drag optimization using Munk's criterion for planar wings.**

$$C_{B,i}=\frac{-4}{3Sb}\left\{s_i^3+s_{i-1}^3+4s_i^2(y_i\cos\phi_i+z_i\sin\phi_i)\right.$$
$$+2s_{i-1}^2(y_{i-1}\cos\phi_{i-1}+z_{i-1}\sin\phi_{i-1})+2s_is_{i-1}(y_i\cos\phi_i$$
$$\left.+z_i\sin\phi_i)+2(s_i+s_{i-1})\sum_{j=i+1}^{N}s_j(y_j\cos\phi_j+z_j\sin\phi_j)\right\} \tag{20}$$

Explicit expressions for derivatives of $C_D$ with respect to $(\gamma_i/U)$ have been developed and reported in Ref. 14. A simpler, equivalent procedure that has since been developed is to rewrite Eq. (9), in matrix form as

$$C_D=2\sum_{i=1}^{N}\sum_{j=1}^{N}C_{D,ij}=\frac{\gamma}{U}^T[A]\frac{\gamma}{U} \tag{21}$$

where $(\gamma/U)^T$ denotes transpose of the column vector $(\gamma/U)$ and $[A]$ is an $N\times N$ matrix. Individual elements of $[A]$ are

$$A_{ij}=\frac{2}{S}\left\{\frac{1}{4}\left(I_{3ij}-I_{4ij}-I_{5ij}+I_{6ij}+I_{3i-1j}-I_{4i-1j}+I_{5i-1j}\right.\right.$$
$$-I_{6i-1j}+I_{3i-1j-1}+I_{4i-1j-1}+I_{5i-1j-1}+I_{6i-1j-1}+I_{3ij-1}$$
$$+I_{4ij-1}-I_{5ij-1}-I_{6ij-1}\left.\right)+\frac{3}{8}s_i\left(I_{1ij}-I_{2ij}+I_{1ij-1}\right.$$
$$\left.+I_{2ij-1}\right)+\frac{1}{8}s_{i-1}\left(I_{1i-1j}-I_{2i-1j}+I_{1i-1j-1}+I_{2i-1j-1}\right)$$
$$+\frac{1}{2}s_{i-1}\left(I_{1ij}-I_{2ij}+I_{1ij-1}+I_{2ij-1}\right)+\frac{1}{2}\left(s_i+s_{i-1}\right)$$
$$\left.\sum_{k=i+1}^{N}\left(I_{1kj}-I_{2kj}+I_{1kj-1}+I_{2kj-1}\right)\right\} \tag{22}$$

From this form of the equation for the induced drag coefficient plus Eqs. (18-20) a system of $N+2$ linear equations has been written for the $N$ $\gamma_i$ values subject to the $C_L$ and one of the $C_m$ or $C_B$ constraints. Each of the first $N$ of these equations is of the form

$$\sum_{j=1}^{N}\left(A_{ij}+A_{ji}\right)\frac{\gamma_i}{U}+\lambda_1C_{L,i}+\lambda_2C_{m,i}+\lambda_3C_{B,i}=0,\ i=1,\ldots,N \tag{23}$$

The last three equations are

$$\sum_{i=1}^{N}C_{L,i}\frac{\gamma_i}{U}-C_L=0 \tag{24}$$

and either

$$\sum_{i=1}^{N}C_{m,i}\frac{\gamma_i}{U}=0 \tag{25}$$

or

$$\sum_{i=1}^{N}C_{B,i}\frac{\gamma_i}{U}-C_B=0 \tag{26}$$

As with the Munk criterion technique, once the $\gamma_i$ values have been obtained, $\Gamma$ is calculated from Eqs. (4-8) and $C_D$ is evaluated from Eq. (21).

In both optimization techniques, special treatment is required in all equations at the wing tip of each planform. This is because the $N$ unknown $\gamma_i/U$ values have been numbered sequentially from tip to root on the first planform, followed by the $\gamma_i/U$ values, numbered tip to root on the second planform. Essentially, all terms subscripted as $(i+1)$ must be omitted from Eqs. (9,10-12), and (16) at the root of each planform, while all $(i-1)$ subscripted terms must be omitted at the tip of each planform in Eqs. (18-22). Also, since the bound circulation values are zero at each wing tip, the summations of bound circulation terms in Eqs. (8,10-12), and (18-22) must include only $i$ values on the current planform. Further, as discussed in Ref. 8 for the case of a fence located inboard of the wing tip, the wake vorticity shed by the fence must be included in the wing bound circulation inboard of the fence.

## Comparisons of Trefftz Plane Theory with Exact Solutions

The two drag minimization techniques have been compared with some existing exact solutions for both planar and nonplanar wings in Ref. 14. Figures 2-5 have been taken from that report. In Fig. 2, the induced drag efficiency parameter $k$ for a planar isolated wing calculated using both optimization

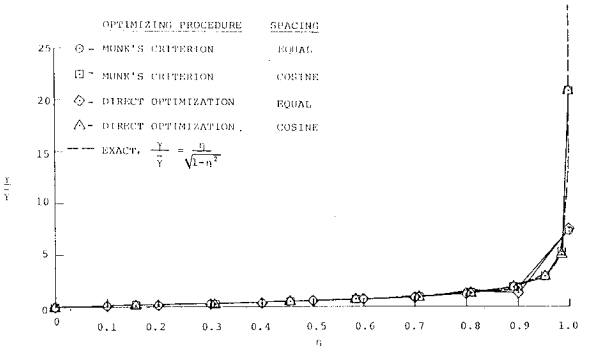


**Fig. 3 Effect of optimizing procedure and spacing on the wake strength for planar wings, $N=10$.**

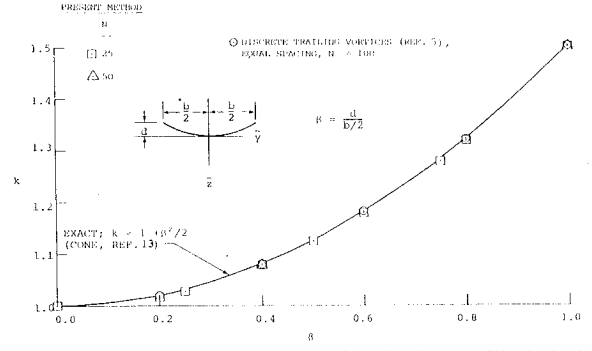


**Fig. 4 Induced drag efficiency factor for circular arc dihedral wings.**

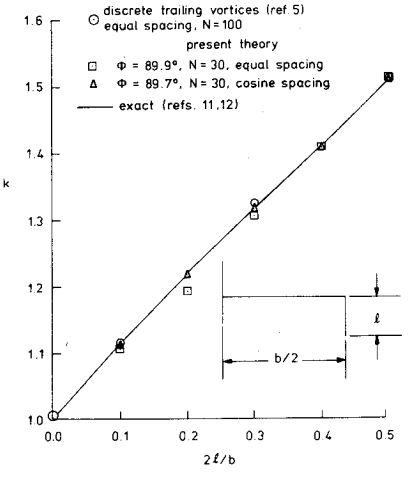


**Fig. 5 Induced drag efficiency for a wing with vertical endplates.**

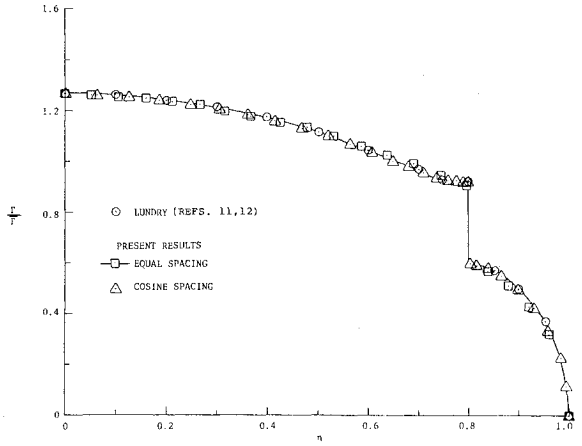


**Fig. 6 Bound circulation distribution for a flat wing with a vertical fence designed for minimum induced drag, $l/(b/2) = 0.125$.**

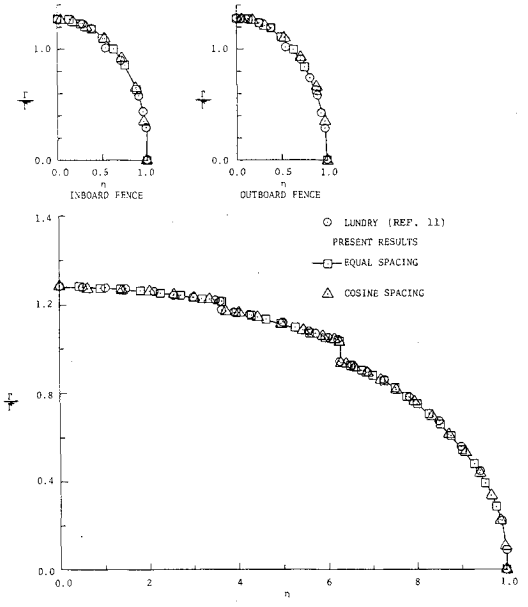


**Fig. 7 Bound circulation distribution for a flat wing with two vertical fences designed for minimum induced drag, $l/(b/2) = 0.10$.**

techniques for the present theory is compared with a discrete vortex wake theory developed by J.R. Tulinius, B.B. Gloss, and J.L. Thomas of NASA Langley Research Center, using the method of Ref. 5. Here $k$ is defined as the ratio of the exact induced drag for a planar wing of equal span to the calculated induced drag. Errors of $k$ values for the present advanced wake model and equal segment spacing are four to five times smaller than those for the discrete vortex wake model using the same number of unknowns. Accuracy of the present method is improved further by using a cosine spacing of the wake segments, with the smallest wake panels at the wing tip. Induced drag efficiency values obtained for the two optimization techniques agree very well. The calculated $\gamma$ distribution for a flat wing is compared with the exact result in Fig. 3. Smaller wake segments (i.e., cosine spacing) near the wing tip again greatly improves the quality of the solution. As in Fig. 2, solutions for the two optimization techniques are in good agreement.

As a sample comparison of the present theory with a nonplanar exact solution by Cone,[13] Fig. 4 displays $k$ values for a series of wings having spanwise camber such that they form portions of a circular arc. The parameter $\beta = 2d/b$ corresponds to a flat wing at $\beta = 0$ and a semicircle at $\beta = 1.0$. Solutions shown have been obtained using the Munk criterion optimization procedure. Here, induced drag efficiencies fall

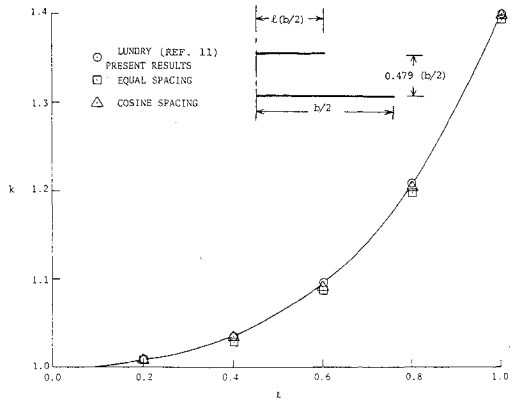


**Fig. 8 Induced drag efficiency factor for biplane with vertical separation of 0.479 times bottom wing span for varying top wing span.**

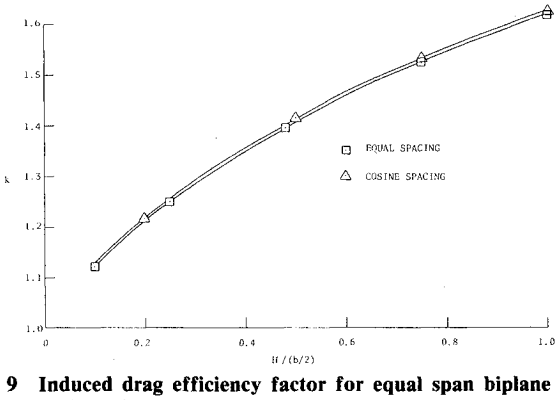


**Fig. 9 Induced drag efficiency factor for equal span biplane with varying vertical wing separation.**

on the exact curve for 25 or 50 equal-sized panels. Figure 5 shows a similar comparison with an exact solution by Lundry and Lissaman[10] for a planar wing with a vertical endplate. The endplate $\phi$ for the current results is not exactly 90 deg to avoid numerical difficulties. Solutions for $k$ for 30 cosine spaced wake panels agree with the exact solution as well as solutions using 100 equal-spaced discrete trailing vortices and the method of Ref. 5. The reason for the relatively large error at $l/(b/2) = 0.2$ for 30 equally spaced panels is not known.

Recently obtained solutions for planar wings with nearly vertical fences are compared in Figs. 6 and 7 with exact solutions given by Lundry.[11,12] The bound circulations, calculated as described in the theoretical development from the $\gamma$ values, are the same as those given by Lundry. Note the jumps in bound circulation which occur at the fence-wing intersections. Although not shown in this paper, the $k$ values for these wings agree with those given by Lundry to five significant figures.

Induced drag efficiency parameter values for a biplane, whose upper wing span varies, are compared with another exact solution due to Lundry[11] in Fig. 8. The current Munk criterion solution with cosine-spaced wake panels agrees well with the exact result. In Fig. 9, two sets of solutions employing Munk's criterion are shown for a biplane where both wings are of equal span, but with varying gap. The $k$ values are seen to increase as the gap increases. The computer program used to generate these results has been documented in a user's manual in Ref. 16.

## Modified Design Code Structure

This higher order Trefftz plane induced drag minimization routine has been joined with an existing vortex lattice subsonic linear theory wing design computer code developed by Lamar.[1] The original wing design program showed evidence

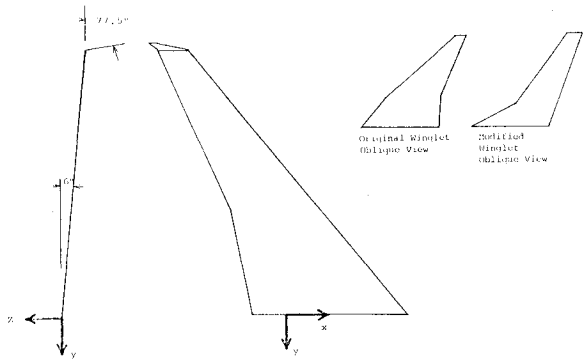

Fig. 10 Planview of subsonic transport-type wing, fitted with winglets.

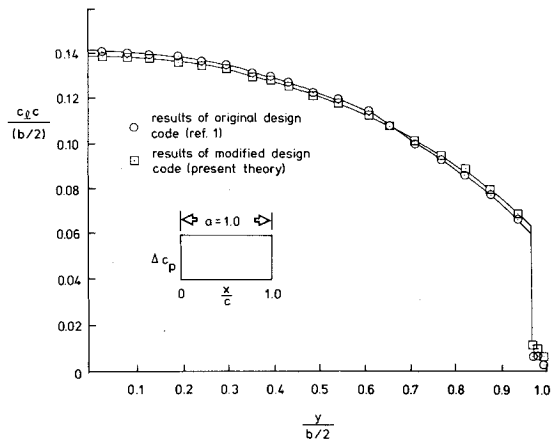


Fig. 11 Spanwise load distribution for wing/winglet configuration designed for minimum induced drag, $M = 0.8$, $C_L = 0.5$, $a = 1.0$.

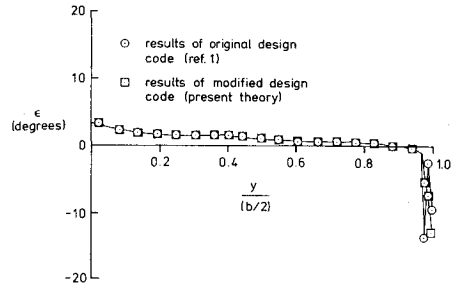


Fig. 12 Incidence distribution for wing/winglet configuration designed for minimum induced drag, $M = 0.8$, $C_L = 0.5$, $a = 1.0$.

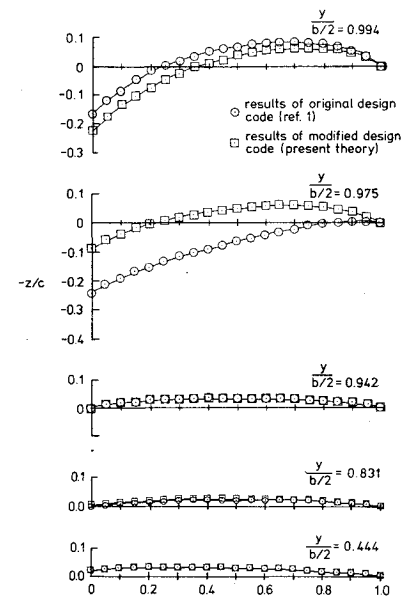


Fig. 13 Representative camber shapes for wing/winglet configuration designed for minimum induced drag, $M = 0.8$, $C_L = 0.5$, $a = 1.0$.

of errors in the induced velocities in regions where changes in dihedral occurred, partly resulting from inaccurate spanloads due to a requirement of equal spacing of the discrete trailing vortices in the original code. However, the current theory minimizes such problems in farfield calculations. Replacing the discrete vortex wake model of Ref. 1 with the current higher order farfield theory provides more accurate span loads, which are then linearly interpolated for the nearfield vortex lattice aerodynamic representation. The modified design code thus consists of the original nearfield vortex lattice geometry program, the Trefftz plane constrained drag minimization program using the current higher order theory and the direct optimization technique developed in this paper, and a third program, unmodified from the original code, where the camber surfaces required to achieve minimum induced drag are computed by spline integration of the local surface slopes obtained from the vortex lattice nearfield solution for the assumed NACA a-series chord loading functions and the farfield optimum span load. Details of the vortex lattice theory and accuracy of the method as currently implemented are given in Refs. 1 and 2. In particular, the same nearfield lattice geometry, AIC expressions and control point locations are used in both codes. Solution for the optimized camber shapes, then, is determined by a direct method in the nearfield after the spanload has been obtained, also directly, in the Trefftz plane.

## Wing/Winglet Design

In Fig. 10, the planform is shown for a wing/winglet configuration, which was one of the examples discussed in Ref. 1. Comparisons between results of the modified design code and the earlier code for this transport-type wing are shown in Figs. 11-13. A rectangular chord loading has been assumed in both theories. There are noticeable differences between the two theories for the calculated spanloads (Fig. 11) and twist distribution (Fig. 12) in the vicinity of the junction between the wing and winglet. Figure 13 compares the designed camber shapes for this planform, which differ significantly only on and near the winglet. The twist distribution and camber shapes on the winglet for the modified code are smoother and are believed to be more accurate. However, the winglet is still highly cambered and such a design may not be practical. Further, boundary layer separation due to recompression after locally supercritical regions on the winglet may significantly degrade performance. These results have been obtained using the direct optimization procedure; an identical design has also been obtained using Munk's criterion for this single planform.

The modified code has also been used for the design of a similar wing/winglet planform, having the same wing planform and winglet tip chord, but with the lower 25% of the new winglet highly swept, $\Lambda = 62.2$ deg (see Fig. 10). The resulting design at $M = 0.8$ and $C_L = 0.5$ is very similar to that shown in Figs. 11-13. This design, with the addition of a constant NACA 64 A 008 thickness distribution[17] on both the wing and winglet, has been analyzed using the Hess potential flow code.[18] Results indicate there are slightly supercritical regions only at the root of the winglet design surface. The modified winglet planform has been chosen using the design criteria recommended by Whitcomb.[19]

However, the resulting cambered, twisted winglet is contrary to the recommendations of Ref. 19 where, based upon a series of wind tunnel tests, optimal winglets are found to be

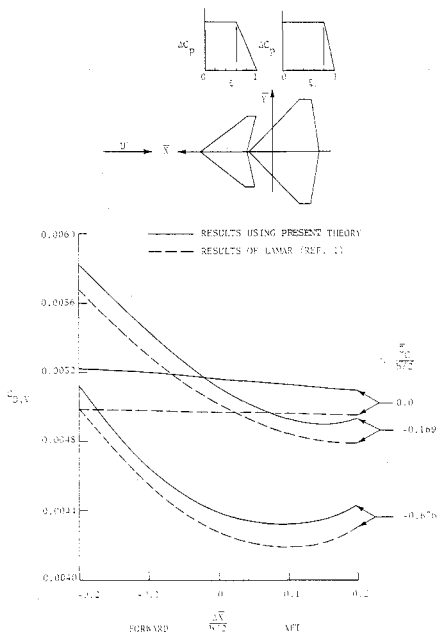


**Fig. 14 Induced drag for wing/canard configuration for various moment trim points and vertical separations, $M=0.3$, $C_L=0.2$.**

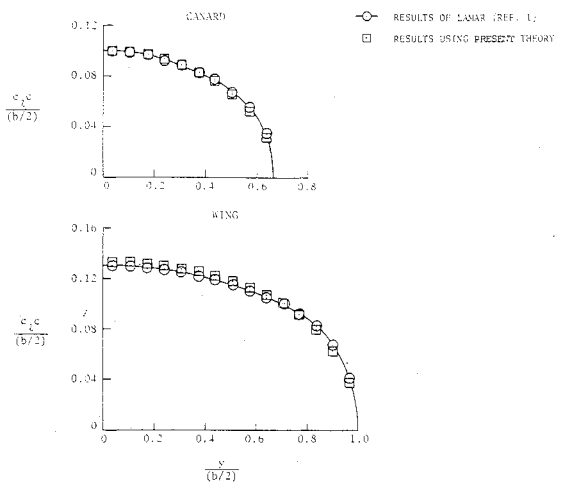


**Fig. 15 Spanwise load distribution for trimmed wing/canard configuration, $M=0.3$, $C_L=0.2$, $\Delta x/(b/2)=0.0$, $z_c/(b/2)=-0.676$.**

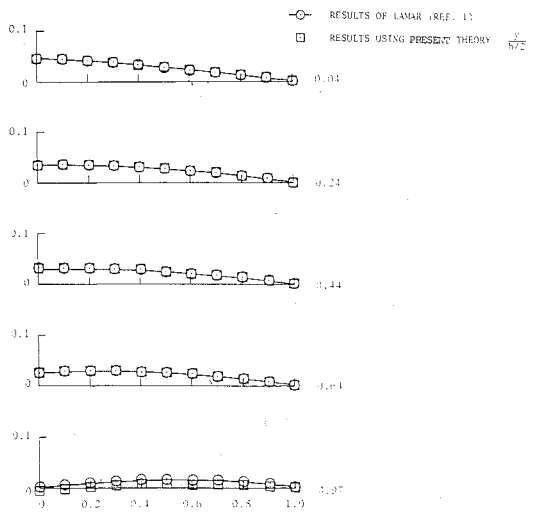


**Fig. 16 Wing camber shapes for trimmed wing/canard configuration, $M=0.3$, $C_L=0.2$, $\Delta x/(b/2)=0.0$, $z_c/(b/2)=-0.676$.**

untwisted with a uniform toe-out angle. In an attempt to assess the practicality of the current design methods, wind tunnel models of the wing/winglet designs using both design codes are currently being constructed for testing in the NASA Langley Research Center $7\times10$ ft high speed wind tunnel. Both force and pressure measurements are planned, as well as wing root bending moment measurements. The details of the design considerations for these models are given in Ref. 20.

## Wing/Canard Design

A multiple planform design is summarized in Figs. 14-16. The wing and canard planforms are shown in Fig. 14. Both surfaces have $\phi=0$ deg. Also shown are the chord loading shapes; $a=0.6$ on the canard, while $a=0.8$ on the wing. All results shown are at $C_L=0.2$ and $M=0.3$. The vertical separation between the two planforms and the moment trim point have been varied.

In Fig. 14, the calculated induced drag obtained using the present design code is compared with results reported in Ref. 1. Drag levels computed with the present theory are consistently higher than those of Ref. 1. A similar behavior may be noted for $C_D$ values for a single planar wing, as shown in Fig. 2. That is, the lower values of $k$ for the present theory correspond to higher, more accurate values of $C_D$. Spanloads on wing and canard are compared in Fig. 15, for a vertical separation of $z_c/(b/2)=-0.676$ and an unshifted trim point. The wing spanload is slightly higher near the wing centerline using the present code, while very little difference can be seen between solutions on the canard. Camber shapes for this one example case, seen in Fig. 16, are identical for the two solutions over the major portion of the wing. There are noticeable but slight differences in the vicinity of the wing tip.

## Conclusion

A Trefftz plane farfield analysis has been developed for a two-dimensional advanced panel model of the undistorted interacting wakes of multiple subsonic planforms. In the current wake model, the vortex strength has been assumed to vary in the spanwise direction piecewise linearly.

The development of two drag minimization techniques has been outlined: first, use of Munk's criterion for wings constrained only as to the total lift generated; and second, a direct optimization technique. The second technique is applicable to more practical constrained optimization problems where, for example, the wing root bending moment is to be limited or the configuration must be trimmed.

Convergence of the calculated drag has been found to be approximately four times faster than for a discrete trailing vortex wake model for equally spaced wake panels. Cosine-spaced wake panels dramatically improve this convergence and have been seen to improve greatly the representation of the wake vortex sheet strengths near the tip of a planar wing.

The theory has been compared with several nonplanar wing configurations for which exact solutions are available. Generally, agreement with the exact induced drag is within 1% or better for 25 to 50 unknown wake strengths.

The direct optimization technique and code have been mated with an existing vortex lattice wing design code. A comparison has been made between the designed spanloads, incidence angles, and camber surfaces for design of a transport-type wing fitted with winglets. The modified design code results differ significantly on the winglet and on the wing in the vicinity of the wing/winglet intersection. As a test of the effectiveness of the two design codes, the wing/winglet wind tunnel models designed using both codes are currently under construction for future force and pressure tests. A second example of a planar wing/canard design has been presented, where the designed spanloads, incidence, and camber surfaces differ very little for the two theories, while the present theory consistently gives a slightly higher drag value. From these two design examples, it is concluded that the present theory gives

significantly different design camber shapes only in the vicinity of changes of planform dihedral. However, the wind tunnel results will be necessary to assess which design code is actually preferable, since it is possible that the current, more accurate spanloads, when interpolated in the nearfield vortex lattice representation, do not result in significantly improved designs.

## Acknowledgment

This research has been sponsored by the NASA Langley Research Center, under Grant NSG-1357.

## References

[1] Lamar, J.E., "A Vortex Lattice Method for the Mean Camber Shapes of Trimmed Noncoplanar Planforms with Minimum Vortex Drag," NASA TN D-8090, June 1976.

[2] Margason, R.J. and Lamar, J.E., "Vortex-Lattice FORTRAN Program for Estimating Subsonic Aerodynamic Characteristics of Complex Planforms," NASA TN D-6142, 1971.

[3] Feifel, W.M., "Optimization and Design of Three Dimensional Aerodynamic Configurations of Arbitrary Shape by a Vortex Lattice Method," NASA SP-405 presented at Vortex-Lattice Utilization Workshop, NASA Langley Research Center, Hampton, Va., May 17-18, 1976.

[4] Blackwell, J.A., Jr., "Numerical Method to Calculate the Induced Drag or Optimum Loading for Arbitrary Non-Planar Aircraft," NASA SP-405 presented at Vortex-Lattice Utilization Workshop, NASA Langley Research Center, Hampton, Va., May 17-18, 1976.

[5] Tulinius, J., Clever, W., Niemann, A., Dunn, K., and Gaither, B., "Theoretical Prediction of Airplane Stability Derivatives at Subcritical Speeds," NASA CR-132681, 1975.

[6] Clever, W.C., "Spanwise Variation of Potential Form Drag," NASA CR-145180, May 1977.

[7] Goldhammer, M.I., "A Lifting Surface Theory for the Analysis of Nonplanar Lifting Systems," AIAA Paper 76-16 presented at 14th Aerospace Sciences Meeting, Washington, D.C., Jan. 26-28, 1976.

[8] Loth, J.L. and Boyle, R.E., "Optimum Loading on Non-Planar Wings at Minimum Induced Drag," Aerospace Engineering TR-19, West Virginia University, Morgantown, Aug. 1969.

[9] Munk, M.M., "The Minimum Induced Drag of Airfoils," NACA TR 121, 1921.

[10] Lundry, J.L. and Lissaman, P.B.S., "A Numerical Solution for the Minimum Induced Drag of Non-Planar Wings," *Journal of Aircraft,* Vol. 5, Jan.-Feb. 1968, pp. 17-22.

[11] Lundry, J.L., "A Numerical Solution for the Minimum Induced Drag and the Corresponding Loading of Non-Planar Wings," NASA CR-1218, 1968.

[12] Lundry, J.L., "A Numerical Solution for the Minimum Induced Drag and the Corresponding Loading of Non-Planar Wings, I – User's Manual for Computer Program 55VD and II – Descriptive Manual for Computer Program 55VD," Supplement to NASA CR-1218, Nov. 1968.

[13] Cone, C.D., Jr., "The Theory of Induced Lift and Minimum Induced Drag for Non-Planar Lifting Systems," NASA Technical Rept. R-139, 1962.

[14] Kuhlman, J.M., "Numerical Optimization Techniques for Bound Circulation Distribution for Minimum Induced Drag of Non-Planar Wings: Basic Formulations," NASA CR-3154, June 1979.

[15] *MACSYMA Reference Manual,* Version 8, The Math Lab Group, Project MAC, M.I.T., Cambridge, Mass., Nov. 1975.

[16] Kuhlman, J.M. and Ku, T.J., "Numerical Optimization Techniques for Bound Circulation Distribution for Minimum Induced Drag of Non-Planar Wings: Computer Program Documentation," NASA Technical Progress Rept., Grant NSG 1357, Nov. 1979.

[17] Abott, I.H. and Von Doenhoff, A.E., *Theory of Wing Sections,* Dover Publications, New York, 1959.

[18] Hess, J.L., "Calculation of Potential Flow About Arbitrary Three Dimensional Lifting Bodies," Rept. MDC J5679-01, McDonnell-Douglas Corp., 1972.

[19] Whitcomb, R.T., "A Design Approach and Selected Wind-Tunnel Results at High Subsonic Speeds for Wing-Tip Mounted Winglets," NASA TN D-8260, 1976.

[20] Kuhlman, J.M., "Optimized Aerodynamic Design Process for Subsonic Transport Wing Fitted with Winglets," NASA CR 159180, Dec. 1979.